Longitudinal detection of ferromagnetic resonance using x-ray transmission measurements

G. Boero,[1,a)] S. Rusponi,[1] J. Kavich,[2] A. Lodi Rizzini,[2] C. Piamonteze,[3] F. Nolting,[3] C. Tieg,[4] J.-U. Thiele,[5] and P. Gambardella[2,6]
[1]*Ecole Polytechninque Federale de Lausanne (EPFL), CH-1015 Lausanne, Switzerland*
[2]*Centre d'Investigació en Nanociència i Nanotecnologia (ICN-CSIC), E-08193 Bellaterra, Barcelona, Spain*
[3]*Swiss Light Source (SLS), Paul Scherrer Institut, CH-5232 Villigen, Switzerland*
[4]*European Synchrotron Radiation Facility (ESRF), F-38043 Grenoble, France*
[5]*Seagate Technology, 47010 Kato Road, Fremont, California 94538, USA*
[6]*Institució Catalana de Recerca i Estudis Avançats (ICREA), E-08100 Barcelona, Spain*

(Received 7 September 2009; accepted 3 November 2009; published online 3 December 2009)

We describe a setup for the x-ray detection of ferromagnetic resonance in the longitudinal geometry using element-specific transmission measurements. Thin magnetic film samples are placed in a static magnetic field collinear with the propagation direction of a polarized soft x-ray beam and driven to ferromagnetic resonance by a continuous wave microwave magnetic field perpendicular to it. The transmitted photon flux is measured both as a function of the x-ray photon energy and as a function of the applied static magnetic field. We report experiments performed on a 15 nm film of doped Permalloy ($Ni_{73}Fe_{18}Gd_7Co_2$) at the L_3/L_2-edges of Fe, Co, and Ni. The achieved ferromagnetic resonance sensitivity is about 0.1 monolayers/$\sqrt{\text{Hz}}$. The obtained results are interpreted in the framework of a conductivity tensor based formalism. The factors limiting the sensitivity as well as different approaches for the x-ray detection of ferromagnetic resonance are discussed. © *2009 American Institute of Physics.* [doi:10.1063/1.3267192]

I. INTRODUCTION

The recently introduced x-ray detection of ferromagnetic resonance opened the possibility to perform element-specific magnetic resonance studies.[1–17] Element sensitivity is obtained by choosing the x-ray photon energy corresponding to a core-to-valence band transition of the atom under investigation. The relatively large separation between the absorption lines of the different elements at the x-ray energies of interest as well as the x-ray absorption line shape dependence on the type and position of neighbor atoms allows one to study the magnetic properties of each element separately in well defined environments. Successful experiments of x-ray detection of ferromagnetic resonance (XFMR) have been carried out on metal films and multilayers [$Ni_{80/81}Fe_{20/19}$ (Refs. 2, 5, 9, and 12), $Ni_{72}Fe_{18}Gd_{10}$ (Ref. 16), $Ni/Ni_{80}Fe_{20}$ (Ref. 13), $Ni_{80}Fe_{20}/Cu/Co$ (Ref. 1), $Ni_{81}Fe_{19}/Cu/Co_{93}Zr_7$ (Refs. 6, 8, 9, and 17), $Co_{93}Zr_7/(Ni_{81}Fe_{19})_{99}Tb_{1\%}$ (Ref. 9), $Co_{90}Fe_{10}/Ru/Ni_{81}Fe_{19}$ (Refs. 14 and 15)] as well as oxides [$Y_3Fe_5O_{12}$ (Refs. 4, 10, 11, and 16), $Gd_1Y_2Fe_5O_{12}$ (Ref. 13), $Y_{1.3}La_{0.47}Lu_{1.3}Fe_{4.84}O_{12}$ (Ref. 10)], using either fluorescence,[2–4,8,10,11,13,16] reflectivity,[2,8] or transmission measurements.[1,5,6,8,9,12,14,15,17]

Ferromagnetic resonance signals have been observed at energies from 500 eV to 7 keV on the following atoms: Fe (L_3/L_2-edges and K-edge), Ni (L_3/L_2-edges), Co (L_3/L_2-edges), Gd (M_4/M_5-edges), Y (L_3/L_2-edges), O (K-edge), and Tb (M_5-edge). These experiments allowed element-specific studies of the magnetization precession in ferromagnetic[2,8,9] and ferrimagnetic[3,10,11,13,16] compounds as well as measurements of the relative phase and precession angle of the magnetization in coupled metal layers.[6,8,9,14,15,17]

XFMR experiments have revealed, e.g., the precession of induced magnetic moments of nonmagnetic species such as Y and O in the ferrimagnetic oxide $Y_3Fe_5O_{12}$.[11,16] Further, it has been pointed out that XFMR may potentially be used to quantitatively determine dynamic changes of the spin and orbital magnetization using the x-ray magnetic circular dichroism (XMCD) sum rules.[2,10,11,16,17] Most XFMR measurements to date have been carried at fixed x-ray photon energy. Recently, however, x-ray absorption spectra have been measured with microwave excitations in magnetic resonance conditions over an entire absorption edge, opening an unconventional possibility to apply the sum rules.[16,17]

In general, XFMR can be performed using either time-resolved or time-invariant methods. Time-resolved measurements have been reported in Refs. 1, 2, 5, 6, 8, 9, 12, 14, and 15. The time resolution is obtained by taking advantage of the bunch structure of the x-ray photon beam. A pulsed or continuous wave excitation, phase locked and time delayed with respect to the photon bunches repetition frequency, is used to excite the magnetization precession. By measuring the variation of the time-averaged photon flux (i.e., the dc component) impinging on the photodiode at different delay times it is possible to measure the magnetization free precession decay (for pulsed excitation) or the magnetization steady-state precession (for continuous wave excitation). Since the time resolution is obtained by measuring with different delays (such as in an "equivalent time" sampling oscilloscope), a photodiode detector with response time shorter

a)Electronic mail: giovanni.boero@epfl.ch.

than the magnetization precession period is not required. True "real-time" experiments would require a fast detector and a photon bunch repetition frequency at least two times larger than the precession frequency.

In the time-invariant method[3,13,16] described in this paper, the temporal structure of the photon beam (repetition frequency, bunch duration) has no practical influence on the obtained results. As demonstrated by the basic model presented in Sec. II, the measured quantity in our configuration with the photon beam propagation direction collinear with the static magnetic field direction is the variation of the magnetization component along the static magnetic field direction, equivalent to an x-ray based *longitudinal* detection of magnetic resonance. The signal-to-noise ratio achievable in transmission experiments is evaluated in Sec. III. Section IV describes in detail the experimental setup. The experimental results obtained on a 15 nm thick sample of doped Permalloy are presented in Sec. V. A brief discussion concerning future opportunities in the field of x-ray detection of magnetic resonance is given in Sec. VI.

The original contributions of this work are the following: (1) the detailed description of an experimental apparatus for the x-ray detection of ferromagnetic resonance in transmission, (2) the introduction of a basic model based on the conductivity tensor formalism for the description of some aspects of the x-ray detection of ferromagnetic resonance, and (3) the comparison of the obtained experimental results with the proposed basic model, with quantitative considerations about the measured signal amplitude, noise, and sensitivity.

II. BASIC THEORETICAL CONSIDERATIONS

Resonant soft x-ray magneto-optical properties are usually described in the formalism of the optical conductivity (or dielectric) tensor or in that of the resonant atomic scattering factor. The equivalence between the two formalisms is discussed in Ref. 18. Here we develop a basic framework for the understanding of some aspects of the x-ray detection of ferromagnetic resonance based on the conductivity tensor formalism. In particular, we will obtain expressions for the x-ray absorption coefficients as a function of the conductivity tensor elements, magnetization precession angle, and beam polarization. A more exhaustive description of XFMR should include also the computation of the x-ray energy dependence of the conductivity tensor elements and of the magnetization dynamics. A detailed treatment of the uniform precession mode within the Landau–Lifschitz–Gilbert approach in connection with XFMR has been presented in Ref. 7.

Let us assume that the sample is placed in a magnetic field $\mathbf{B}(t)$ given by the superposition of a static field $\mathbf{B}_0$ along the $\hat{\mathbf{z}}$-axis and of a microwave (MW) field $\mathbf{B}_1$ along the $\hat{\mathbf{x}}$-axis, i.e., $\mathbf{B}(t)=B_0\hat{\mathbf{z}}+B_1\cos(\omega_{\mathrm{MW}}t)\hat{\mathbf{x}}$. If the static magnetic field is set equal to the ferromagnetic resonance condition,[19] the sample magnetization $\mathbf{M}$ precesses about its equilibrium direction, which, in the case of negligible magnetocrystalline anisotropy and large B_0 or perpendicular easy axis, coincides with the $\hat{\mathbf{z}}$-axis. The polar precession angle θ

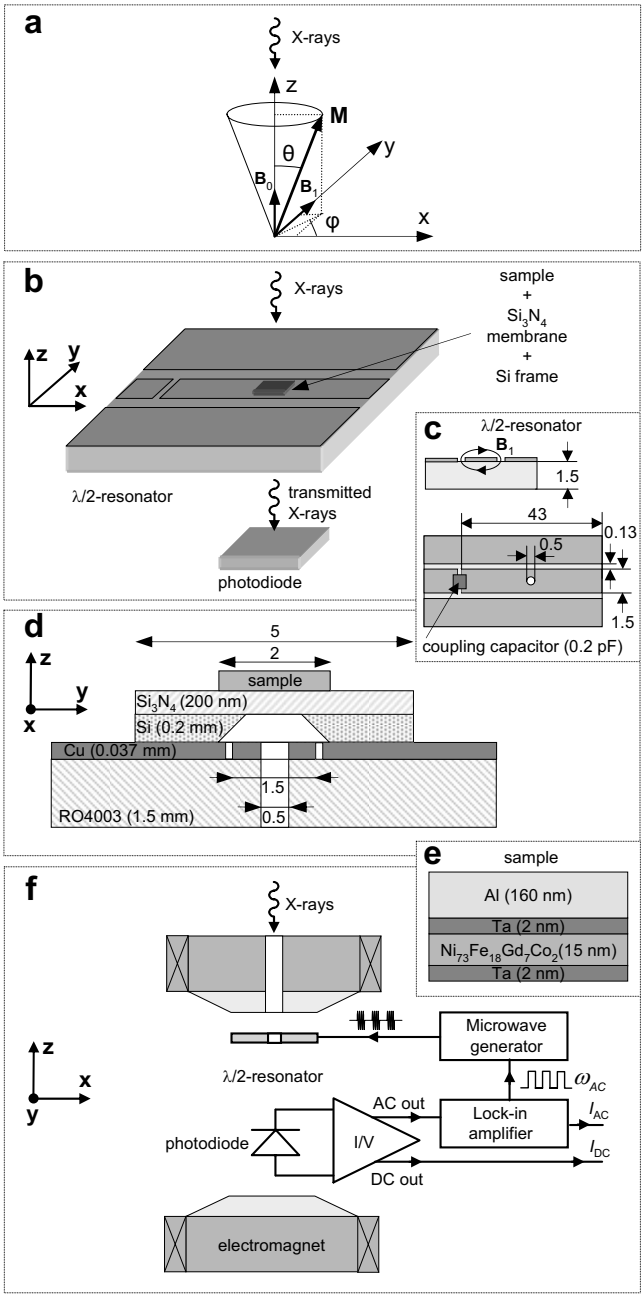

FIG. 1. (a) X-ray beam propagation, static magnetic field $\mathbf{B}_0$, microwave magnetic field $\mathbf{B}_1$, and sample magnetization $\mathbf{M}$ directions. (b) Sample, MW resonator, and photodiode setup. (c) Detail of the MW resonator (dimensions in millimeters, not to scale). (d) Detail of the sample and MW resonator (dimension in millimeters if not otherwise specified, not to scale). (e) Detail of the sample (not to scale). (f) Schematic representation of the experimental setup.

depends on the strength of B_1 until saturation sets in at high MW field.[20] For a uniformly magnetized thin film with out-of-plane $\mathbf{B}_0$, as will be treated here, the resonant static field of the uniform precession mode is $B_R \cong (\omega_{\mathrm{MW}}/\gamma)+\mu_0 M$, where γ is the electron gyromagnetic ratio. The azimuthal angle φ [i.e., the angle between the projection of $\mathbf{M}$ on the $\hat{\mathbf{x}}\hat{\mathbf{y}}$-plane and the $\hat{\mathbf{x}}$-axis, see Fig. 1(a)] varies as $\varphi=\omega_{\mathrm{MW}}t$.

For a sample having cubic or higher symmetry and magnetization direction along $\hat{\mathbf{z}}$, the optical conductivity tensor can be written as[21,22]

$$\boldsymbol{\sigma}^{\mathbf{z}} = \begin{pmatrix} \sigma_{xx} & \sigma_{xy} & 0 \\ -\sigma_{xy} & \sigma_{xx} & 0 \\ 0 & 0 & \sigma_{zz} \end{pmatrix}, \tag{1}$$

where the tensor elements σ_{ij} are complex numbers dependent on the x-ray beam energy, sample composition, and magnetization. For isotropic samples (such as polycrystalline materials), the conductivity tensor for an arbitrary orientation of the magnetization $\mathbf{M}$ takes the form $\boldsymbol{\sigma}=\mathbf{R}\boldsymbol{\sigma}^{\mathbf{z}}\mathbf{R}^{-1}$, where $\mathbf{R}$ is the rotation matrix given by

$$\mathbf{R} = \begin{pmatrix} \cos\varphi\cos\theta & -\sin\varphi & \cos\varphi\sin\theta \\ \sin\varphi\cos\theta & \cos\varphi & \sin\varphi\sin\theta \\ -\sin\theta & 0 & \cos\theta \end{pmatrix}. \tag{2}$$

The photon flux (in photons/s) transmitted through a homogeneous sample of thickness t_s can be written as $I=I_s\exp(-\mu_a t_s)$, where I_s is the photon flux impinging on the sample. The absorption coefficient μ_a (in m^{-1}) can be written as the ratio between the absorbed power per unit of volume[22] and the Poynting vector average amplitude, i.e.,

$$\mu_a = \frac{(1/2)\mathrm{Re}\{(\boldsymbol{\sigma}\mathbf{E})^*\cdot\mathbf{E}\}}{(\varepsilon_0 cE^2/2)} = \frac{1}{\varepsilon_0 cE^2}\mathrm{Re}\{(\boldsymbol{\sigma}\mathbf{E})^*\cdot\mathbf{E}\}, \tag{3}$$

where $\mathbf{E}$ is the x-ray electric field vector, ε_0 the vacuum permittivity, and c the speed of light in vacuum.

Let us assume that the x-ray beam has wave vector $\mathbf{k}\|\hat{\mathbf{z}}$, i.e., it propagates along the magnetization precession axis (see Appendix for the case $\mathbf{k}\|\hat{\mathbf{y}}$). Circularly and linearly polarized x-ray beams propagating along $\hat{\mathbf{z}}$ can be written as

$$\begin{aligned} \mathbf{E}^+ &= -E(1/\sqrt{2})\exp(i\omega_{XR}t)(\hat{\mathbf{x}}+i\hat{\mathbf{y}}), \\ \mathbf{E}^- &= E(1/\sqrt{2})\exp(i\omega_{XR}t)(\hat{\mathbf{x}}-i\hat{\mathbf{y}}), \\ \mathbf{E}^x &= E\exp(i\omega_{XR}t)\hat{\mathbf{x}}, \\ \mathbf{E}^y &= E\exp(i\omega_{XR}t)\hat{\mathbf{y}}, \end{aligned} \tag{4}$$

where $\hbar\omega_{XR}$ is the x-ray photon energy. From the previous equations we have that the measurable absorption $\mu=\mu_a t_s$ is

$$\begin{aligned} \mu^+ &= \alpha(-\cos\theta\,\mathrm{Im}[\sigma_{xy}] + (1/2)(1+\cos^2\theta)\mathrm{Re}[\sigma_{xx}] \\ &\quad + (1/2)\sin^2\theta\,\mathrm{Re}[\sigma_{zz}]), \\ \mu^- &= \alpha(\cos\theta\,\mathrm{Im}[\sigma_{xy}] + (1/2)(1+\cos^2\theta)\mathrm{Re}[\sigma_{xx}] \\ &\quad + (1/2)\sin^2\theta\,\mathrm{Re}[\sigma_{zz}]), \\ \mu^x &= \alpha[(\cos^2\theta+\sin^2\theta\sin^2\varphi)\mathrm{Re}[\sigma_{xx}] \\ &\quad + \sin^2\theta\cos^2\varphi\,\mathrm{Re}[\sigma_{zz}]], \\ \mu^y &= \alpha[(\cos^2\theta+\sin^2\theta\cos^2\varphi)\mathrm{Re}[\sigma_{xx}] \\ &\quad + \sin^2\theta\sin^2\varphi\,\mathrm{Re}[\sigma_{zz}]], \end{aligned} \tag{5}$$

and

$$\begin{aligned} \mu^+ - \mu^- &= -\alpha 2\cos\theta\,\mathrm{Im}[\sigma_{xy}], \\ \mu^x - \mu^y &= \alpha\sin^2\theta\cos 2\varphi(\mathrm{Re}[\sigma_{zz}] - \mathrm{Re}[\sigma_{xx}]), \\ \mu^+ + \mu^- &= \alpha[(1+\cos^2\theta)\mathrm{Re}[\sigma_{xx}] + \sin^2\theta\,\mathrm{Re}[\sigma_{zz}]], \\ \mu^x + \mu^y &= \alpha[(1+\cos^2\theta)\mathrm{Re}[\sigma_{xx}] + \sin^2\theta\,\mathrm{Re}[\sigma_{zz}]], \end{aligned} \tag{6}$$

where $\alpha=(t_s/\varepsilon_0 c)$.

From Eq. (5) we have that, for circularly polarized light propagating along the precession direction $\hat{\mathbf{z}}$, the absorptions $\mu^{\pm}$ are independent on φ. Consequently, measurements with circularly polarized light propagating along the precession axis are not directly sensitive to the time-dependent magnetization precession, and are therefore equivalent to the so-called longitudinal detection of magnetic resonance.[20] On the other hand, measurements with linearly polarized light are sensitive to the magnetization precession if $\mathrm{Re}[\sigma_{zz}] \neq \mathrm{Re}[\sigma_{xx}]$, i.e., for nonzero magnetic linear dichroism.

In order to improve the sensitivity to the small variations of the x-ray absorption intensity induced by MW excitations (see Sec. V), the magnetic field $\mathbf{B}_1$ is square-wave amplitude modulated, i.e.,

$$\mathbf{B}_1(t) = B_1\hat{\mathbf{x}}\cos(\omega_{\mathrm{MW}}t)\left((1/2) + (2/\pi)\sum_{n=1}^{\infty}(1/n)\sin(n\pi/2)\cos(n\omega_{\mathrm{ac}}t)\right), \tag{7}$$

where ω_{ac} is the frequency of the modulating square wave. Neglecting the nanosecond-scale transients at the beginning and at the end of each MW excitation, which is a reasonable assumption for the "steady state precession" experiments reported in this paper, but not for the "free precession decay" experiments reported in Refs. 2, 8, and 14 where the decay after the excitation is actually measured, the angle θ can be written as

$$\theta(t) = \theta\left((1/2) + (2/\pi)\sum_{n=1}^{\infty}(1/n)\sin(n\pi/2)\cos(n\omega_{\mathrm{ac}}t)\right). \tag{8}$$

Consequently, the absorption $\mu^{\pm}(t)$ contains terms at frequency $\omega=(0,\omega_{\mathrm{ac}},2\omega_{\mathrm{ac}},3\omega_{\mathrm{ac}},\ldots)$.

For circularly polarized light and small cone angles, i.e., for $\cos\theta\cong[1-(\theta^2/2)]$ we have that the components at frequencies $\omega=0$ and $\omega=\omega_{\mathrm{ac}}$ are

$$\begin{aligned} \mu^+_{\mathrm{dc}} &= \alpha\{[-1+(\theta^2/4)]\mathrm{Im}[\sigma_{xy}] + [1-(\theta^2/4)]\mathrm{Re}[\sigma_{xx}] \\ &\quad + (\theta^2/4)\mathrm{Re}[\sigma_{zz}]\}, \\ \mu^-_{\mathrm{dc}} &= \alpha\{[1-(\theta^2/4)]\mathrm{Im}[\sigma_{xy}] + [1-(\theta^2/4)]\mathrm{Re}[\sigma_{xx}] \\ &\quad + (\theta^2/4)\mathrm{Re}[\sigma_{zz}]\}, \\ \mu^+_{\mathrm{ac}} &= (\alpha/\pi)\theta^2(\mathrm{Im}[\sigma_{xy}] - \mathrm{Re}[\sigma_{xx}] + \mathrm{Re}[\sigma_{zz}]), \\ \mu^-_{\mathrm{ac}} &= (\alpha/\pi)\theta^2(-\mathrm{Im}[\sigma_{xy}] - \mathrm{Re}[\sigma_{xx}] + \mathrm{Re}[\sigma_{zz}]), \end{aligned} \tag{9}$$

and, hence,

$$\begin{aligned} (\mu^+_{\mathrm{dc}} - \mu^-_{\mathrm{dc}}) &= \alpha\{[-2+(\theta^2/2)]\mathrm{Im}[\sigma_{xy}]\}, \\ (\mu^+_{\mathrm{dc}} + \mu^-_{\mathrm{dc}}) &= \alpha\{[2-(\theta^2/2)]\mathrm{Re}[\sigma_{xx}] + (\theta^2/2)\mathrm{Re}[\sigma_{zz}]\}, \\ (\mu^+_{\mathrm{ac}} - \mu^-_{\mathrm{ac}}) &= \alpha(2/\pi)\theta^2\,\mathrm{Im}[\sigma_{xy}], \end{aligned}$$

$$(\mu_{ac}^{+} + \mu_{ac}^{-}) = \alpha(2/\pi)\theta^2(\mathrm{Re}[\sigma_{zz}] - \mathrm{Re}[\sigma_{xx}]). \quad (10)$$

For small angles θ, we have $(\mu_{dc}^{+} - \mu_{dc}^{-}) \cong -2\alpha\ \mathrm{Im}[\sigma_{xy}]$. Consequently, $(\mu_{dc}^{+} - \mu_{dc}^{-})$ is only marginally different from the "ordinary" magnetic circular dichroism measured in the absence of the MW perturbation. Such difference, for $\theta \leq 10°$ as in our typical experimental conditions, is smaller than 1%. More generally, the dc absorption reflects to a very good approximation the unperturbed x-ray absorption, whereas the ac absorption reveals MW-induced variations of x-ray absorption in a quantitative way.

Since the projection of the magnetization on the $\hat{\mathbf{z}}$-axis decreases at resonance, one might intuitively expect that μ_{ac}^{+} and μ_{ac}^{-} should reflect, respectively, the subtraction or addition of a common small dichroism signal to the total x-ray absorption intensity. However, from the equations above, we have that $(\mu_{ac}^{+} + \mu_{ac}^{-}) = 0$ only if $\mathrm{Re}[\sigma_{zz}] = \mathrm{Re}[\sigma_{xx}]$. This means that reversing the light polarization, the ac absorption $\mu_{ac}^{\pm}$ does not necessarily change its sign and keeps its magnitude constant, as indeed observed in previous experiments.[3,16]

In Eq. (10) we notice that the ac and dc dichroisms have the same dependence on the conductivity tensor elements and that $[(\mu_{dc}^{+} - \mu_{dc}^{-})/(\mu_{ac}^{+} - \mu_{ac}^{-})] \cong -\pi/\theta^2$. This means that the ac and dc dichroisms are predicted to have the same energy dependence (line shape) and that their ratio is a function of the precession angle θ only.

Taking into consideration the synchrotron radiation bunch structure, the photon flux impinging on the sample can be approximated by a pulsed wave, i.e.,

$$I_s^{\pm}(t) = I_s^{\pm} + (2I_s^{\pm}/\pi d)\sum_{n=1}^{\infty}(1/n)\sin(n\pi d)\cos(n\omega_{PB}t), \quad (11)$$

where d, ω_{PB}, and $I_s^{\pm}$ are the duty-cycle, repetition frequency, and time-averaged flux of the photon bunches, respectively. Since the photon flux transmitted through the sample can be written as $I^{\pm}(t) = I_s^{\pm}(t)\exp(-\mu^{\pm}(t))$, $I^{\pm}(t)$ will contain components at frequencies $\omega = (0, \omega_{ac}, 2\omega_{ac}, 3\omega_{ac}, \ldots, \omega_{PB}, 2\omega_{PB}, 3\omega_{PB}, \ldots, \omega_{PB} \pm \omega_{ac}, 2\omega_{PB} \pm \omega_{ac}, \ldots)$.

The photon flux transmitted through the sample is usually measured with an x-ray optimized photodiode.[23] Since the current produced by the photodiode (in A) is linearly proportional to the photon flux reaching the photodiode (in photons/s), with a proportionality factor approximately given by $Q = e(\hbar\omega_{XR}/\varepsilon)$ in C/photon, where e is the electron charge and $\varepsilon \cong 3.6$ eV for silicon photodiodes,[24] we can use the same notation also for indicating the current produced by the photodiode detector.

The current components at $\omega = 0$ and at $\omega = \omega_{ac}$, which we will indicate with $I_{dc}^{\pm}$ and $I_{ac}^{\pm}$, respectively, can be converted into absorption spectra $\mu_{dc}^{\pm}$ and $\mu_{ac}^{\pm}$ using the relation $\mu = -\ln(I/I_s)$. For small θ angles, it follows that $I_{dc}^{\pm} \gg I_{ac}^{\pm}$ and, hence, $\mu_{dc}^{\pm} \cong -\ln(I_{dc}^{\pm}/I_s^{\pm})$ and $\mu_{ac}^{\pm} \cong -(I_{ac}^{\pm}/I_{dc}^{\pm})$.

III. SIGNAL-TO-NOISE RATIO

Let us discuss now the parameters affecting the signal-to-noise ratio in transmission-mode x-ray detection of magnetic resonance. The current measured by the photodiode can be written, more generally than in Sec. II, as $I = QI_s \exp(-(\mu_t + \delta\mu_t)t_s)$, where μ_t is the total absorption coefficient of the sample, and $\delta\mu_t \ll \mu_t$ is the variations of the total absorption coefficients due to the ferromagnetic resonance phenomenon. The total absorption coefficient μ_t can be generally written as $\mu_t = \mu_a + \mu_b$ and its variation as $\delta\mu_t = \delta\mu_a + \delta\mu_b$, where the subscripts a and b indicate, respectively, the particular atom under investigation and the other atoms in the sample (the "background"). The possibility to perform element-resolved ferromagnetic resonance experiments is due to the fact that, at the absorption edges of the atom a, we have $\delta\mu_t \cong \delta\mu_a$. This is a reasonable hypothesis if the atom a is not excessively diluted and/or the investigated absorption edge is sufficiently separated from the absorption edges of the other atoms in the sample.

The useful signal (i.e., the variation of the photodiode current due to the ferromagnetic resonance phenomenon) is given by $\delta I \cong QI_s t_s \delta\mu_a \exp(-\mu_t t_s)$. The noise on the photodiode output current is essentially shot noise, with a root-mean-square value given by $N_{rms} = \sqrt{2e(\hbar\omega_{XR}/\varepsilon)I\Delta f} = \sqrt{2QI\Delta f}$ (see Ref. 25). Consequently, the signal-to-noise ratio is

$$\mathrm{SNR} = \frac{\delta I}{N_{rms}} \cong \sqrt{\frac{QI_s}{2\Delta f}}\exp(-\mu_t t_s/2)t_s\delta\mu_a. \quad (12)$$

The maximum SNR is obtained for $t_s = 2/\mu_t$ and it is given by

$$\mathrm{SNR}(t_s = 2/\mu_a) \cong \frac{1}{2}\sqrt{\frac{QI_s}{\Delta f}}\frac{\delta\mu_a}{\mu_t}. \quad (13)$$

This equation states that, for a given thickness t_s, the signal-to-noise ratio can be improved by increasing the photon flux I_s impinging on the sample and/or the amplitude of the MW field B_1 (which increases θ and, hence, $\delta\mu_a$).

The photon flux can be increased by opening the monochromator slits. However, this reduces the energy resolution and increases the beam size. The upper limit in the photon flux is set by either radiation damage of the sample or beam-induced heating effects, which can be severe in the case of thin specimens used in transmission experiments. State-of-the-art soft x-ray beamlines have a photon flux up to 10^{13} photons/s on the sample, with beam size of the order of $(0.1\ \mathrm{mm})^2 - (1\ \mathrm{mm})^2$. Up to these photon flux densities, we have observed no radiation damage on metallic thin film at x-ray energies from 500–1400 eV. However, at maximum photon flux, heat induced by x-ray absorption was found to decrease the dc dichroism by nearly 100% on 15 nm thick Permalloy films deposited on 100 nm thick Si_3N_4 membranes. This effect can be reduced significantly, well below MW-induced heating, by increasing the heat dispersion from the sample. In our case, we deposited a 160 nm Al layer over the Permalloy film (Sec. IV).

The maximum B_1 is limited by the resonator and sample heating due to the delivered MW power. In order to work at large B_1, efficient sample cooling and/or MW power-to-B_1 conversion have to be implemented. For instance, in the measurements reported in this work (Secs. IV and V), we

operate in stable conditions up to a MW power of about 3 W, corresponding to a sample temperature of 370 K and a B_1 of 0.4 mT at the sample position.

IV. EXPERIMENTAL SETUP

The experiments reported in this paper have been performed at the surface interface microscopy (SIM) beamline of the Swiss Light Source in Villigen, Switzerland. Two undulators operated in series are used to produce circularly polarized beams with a degree of polarization larger than 98%, and a size of $(100\times100\ \mu m^2)$ at the sample position. The x-ray photon bunches have a repetition frequency of 500 MHz, a width of about 35 ps (i.e., a duty-cycle of about 2%), and a time-averaged photon flux $I_s\sim10^{13}$ photons/s (i.e., about 2×10^4 photons/bunch). The energy shift between circularly polarized light of opposite helicity is typically below 0.02 eV.

The experimental end station essentially combines an electromagnet with a vacuum chamber. The latter is separated from the beam line vacuum by a $(500\times500\ \mu m^2\times200$ nm) Si_3N_4 membrane. This membrane allows us to fill the end-station vacuum chamber with He up to a pressure of 200 mbar. The x-ray beam travels for about 400 mm, the distance from the Si_3N_4 membrane to the photodiode detector, through the He gas, with an attenuation of less than 20% at the photon beam energies employed in this work. The presence of He in the chamber improves the cooling of the sample, allowing us to operate at larger MW power. The electromagnet can produce static magnetic fields B_0 up to ±0.8 T, with a pole face diameter of 14 mm and a gap of 10 mm. The poles have a 5 mm hole to allow the passage of the x-ray beam, which has propagation direction collinear with the pole axis and, consequently, with the static magnetic field (see Fig. 1). In the gap between the electromagnet poles, a $\lambda/2$-coplanar waveguide microwave resonator and a silicon photodiode are introduced.

The coplanar resonator is fabricated on a low loss dielectric substrate (RO4003C, Rogers Corporation, USA), having a copper cladding of 34 μm, dielectric constant $\varepsilon_r\cong3.4$, and dissipation factor tan $\delta\cong0.002$. The central line has a width of 1.5 mm and the gap between the central line and the ground plane is 0.13 mm [see Fig. 1(c)]. The length of the resonator is 43 mm. A capacitor of 0.2 pF is used to optimally couple the resonator to the 50 Ω coplanar transmission line. The resonator has a 0.5 mm hole to allow the passage of the x-ray beam. The sample is glued on the resonator as schematically shown in Fig. 1(b). The estimated MW magnetic field B_1 at the sample position is about 0.4 mT for an input power of 3 W at the resonator resonance frequency of 2.17 GHz. This estimation is based on numerical simulation of the microwave field produced by the resonator as well as by conventional paramagnetic resonance measurements of the saturation curve of a 1,1-diphenyl-2-picrylhydrazyl sample. At 3 W input MW power, the sample temperature is about 370 K. For the doped Permalloy sample investigated in this work, the operation at 370 K causes a decrease in the resonance field of about 30 mT (i.e., about 5%) with respect to 300 K, due to a reduction of the saturation magnetization of approximately the same factor. Since the MW power is modulated, the temperature of the sample (and, consequently, also its magnetization) has a component at the modulation frequency with amplitude that depends on the thermal time constant of the sample and the modulation frequency. In our experimental conditions, at a modulation frequency $(\omega_{ac}/2\pi)=13$ kHz, the variation of the magnetization due to this purely thermal effect is about 5% of the variation due to the magnetic resonance effect. The phase of the signal due to this thermal effect is, at modulation frequencies well above the thermal cutting frequency, shifted by $\pi/2$ with respect to the magnetic resonance signal. Consequently, it is efficiently separated from the magnetic resonance signal by the lock-in phase-sensitive detection implemented in our setup. The phase variation of this thermal effect was investigated as a function of the MW modulation frequency, showing that the effective thermal cutting frequency is of the order of 1 Hz.

The photodiode (Canberra-Eurisys IP-300–300-PH-CER) has a diameter of 20 mm and a photon flux-to-photodiode current efficiency $Q\cong e(\hbar\omega_{XR}/\varepsilon)$ at the x-ray energies employed in this work. It is placed at about 2 mm from the sample. The photodiode is connected to a transimpedance amplifier (EG&G 5182) with a dc gain of 10^3 V/A and an ac gain of 10^5 V/A. The amplified ac signal is fed into a lock-in amplifier (EG&G 7265). We define the I_{dc} signal as the signal measured at the dc output of the transimpedance amplifier (bandwidth dc to 0.1 Hz) divided by the transimpedance amplifier dc gain. The I_{ac} signal is defined as the signal measured by the lock-in amplifier set to measure the component at ω_{ac}, divided by the transimpedance amplifier ac gain. The I_{dc} and I_{ac} signals are simultaneously acquired.

The noise observed in the I_{ac} measurements is, within 20%, in agreement with the shot noise $\sqrt{2QI\Delta f}$ discussed in Sec. III. In our experimental conditions, $I\sim300$ μA at the L_3/L_2-edges of Fe, Ni, and Co. This corresponds to a shot noise spectral density of about 0.15 nA/$\sqrt{\text{Hz}}$.

The samples are deposited by dc-magnetron sputtering on silicon nitride/silicon windows (Silson Ltd., U.K.). The windows consist of a $(1\times1\ mm^2\times200$ nm) Si_3N_4 membrane supported by a $(5\times5\ mm^2\times200\ \mu m)$ Si frame. The polycrystalline sample measured in this paper is a stack of different metal layers with composition Al(160 nm)/Ta(2 nm)/$Ni_{73}Fe_{18}Gd_7Co_2$(15 nm)/Ta(2 nm)/Si_3N_4(200 nm). The Gd atoms have been introduced to bring the resonant magnetic field within the field range of our electromagnet (with the magnetic field perpendicular to the thin film surface, undoped Permalloy has a resonant magnetic field at 2 GHz of about 1 T). The Al top layer improves the thermal conduction and the mechanical stability of the membrane, with acceptable degradation of the MW resonator quality factor and x-ray beam intensity. The Ta layer is used to improve adhesion. The transmission in the range 700–900 eV of each layer is approximately Al (90%), Ta (95%), $Ni_{73}Fe_{18}Gd_7Co_2$ (90%), and Si_3N_4 (75%), giving a total transmission larger than 50%. Considering also the Si_3N_4 membrane used to separate the end-station chamber from the beam-line vacuum

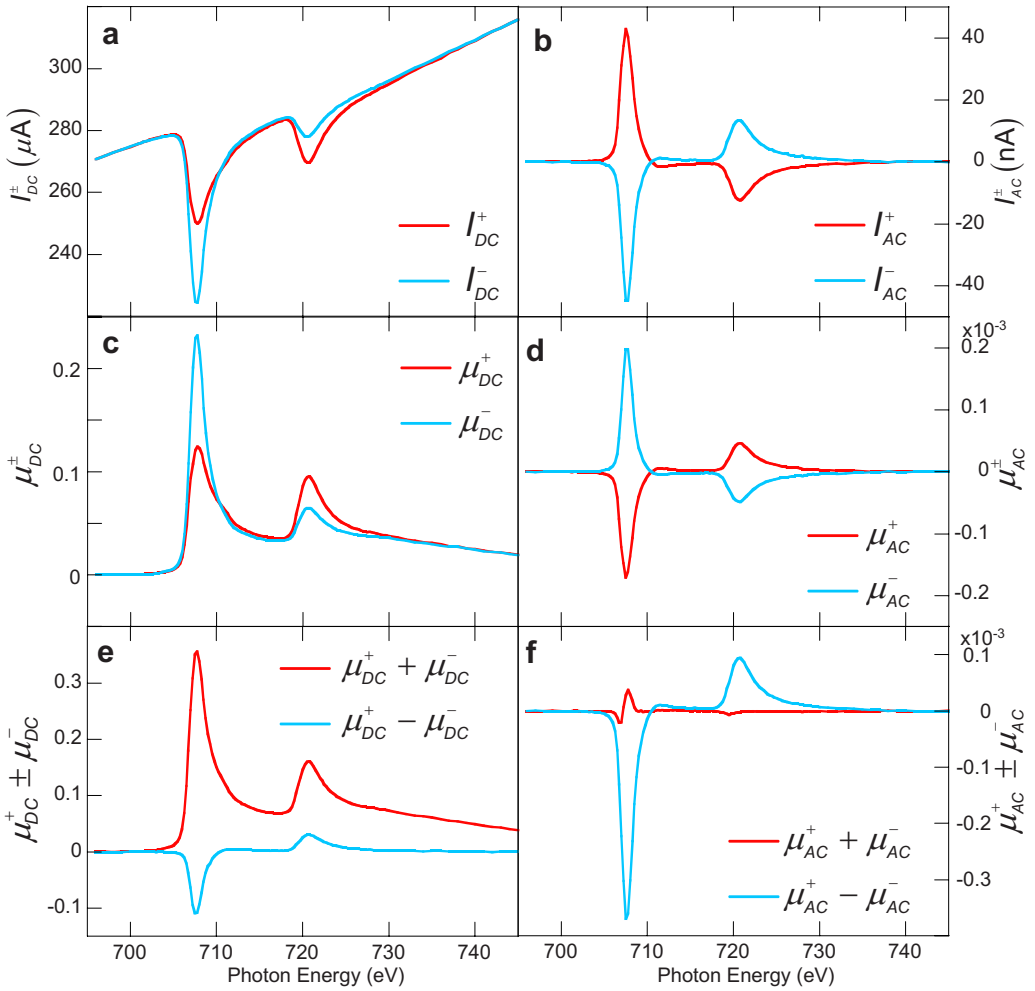

FIG. 2. (Color online) Energy scans at the L_2/L_3-edges of Fe in ferromagnetic resonance condition ($B_0 \cong B_R \cong 0.64$ T). One scan per polarization, 12 min/scan, integration time of 3 s. (a) dc currents, (b) ac currents, (c) dc absorption, (d) ac absorption, (e) sum and difference of the dc absorption, and (f) sum and difference of the ac absorption.

and the He absorption in the end-station chamber, we have a total transmission larger than 40% of the direct beam away from elemental resonances.

V. TRANSMISSION SPECTRA OF DOPED PERMALLOY

In this section, we report in detail the results of measurements performed on the $Ni_{73}Fe_{18}Gd_7Co_2$ sample described in Sec. IV. We have typically adopted the following strategy: (1) preliminary photon energy scans (E-scans) are performed to locate the energy of the maximum of the dc dichroism $\mu^{+}_{dc} - \mu^{-}_{dc}$, (2) preliminary magnetic field scans (B-scans) are performed, with photon energy set at the maximum of the dc dichroism, to locate the resonant field B_R, i.e., the maximum of the ac dichroism $\mu^{+}_{ac} - \mu^{-}_{ac}$, (3) accurate E-scans are performed with $B_0 = B_R$ and, finally, (4) accurate B-scans are performed with the photon energy set to the maximum of the ac dichroism. All measurements reported in this paper have been performed in the following conditions: $B_1 \cong 0.4$ mT, sample temperature $T \cong 370$ K, average photon flux on the sample $I_s \sim 10^{13}$ photons/s, $(\omega_{MW}/2\pi) \cong 2.17$ GHz, and $(\omega_{ac}/2\pi) \cong 13$ kHz.

Figures 2–4 show the E-scans performed at the L_3/L_2-edges of Fe, Co, and Ni, respectively. The current at the output of the photodiode can be written as $I = QI_s \exp(-(\mu_b + \mu_a + \delta\mu_a)t_s) = I_b \exp(-(\mu_a + \delta\mu_a)t_s)$. The dc and ac absorptions are given by $\mu_{dc} \cong -\ln(I_{dc}/I_b)$ and $\mu_{ac} \cong -(I_{ac}/I_{dc})$, where I_{dc} and I_{ac} are the measured dc and ac currents, and I_b is the background current computed by fitting the measured current before the L_3-edge with a straight line. This approximation is made for lack of a better one because the background current is only approximately a straight line. The measured values after the L_2-edge can be used together or as an alternative to the values before the L_3-edge, eventually with a polynomial instead of straight line fitting function. However, this does not guarantee a significantly better accuracy in the determination of the background current I_b. For samples consisting of a single type of atoms deposited on a membrane, the background current can be accurately obtained by measuring the current in the presence of the membrane only.[26] For samples consisting of different atoms, as in our case, an accurate determination of the background is not straightforward (it would require, at least, a series of measurements on samples where each element is alternatively removed, with questionable physical significance due to the substantial changes of the sample properties). The background current I_b as computed above depends

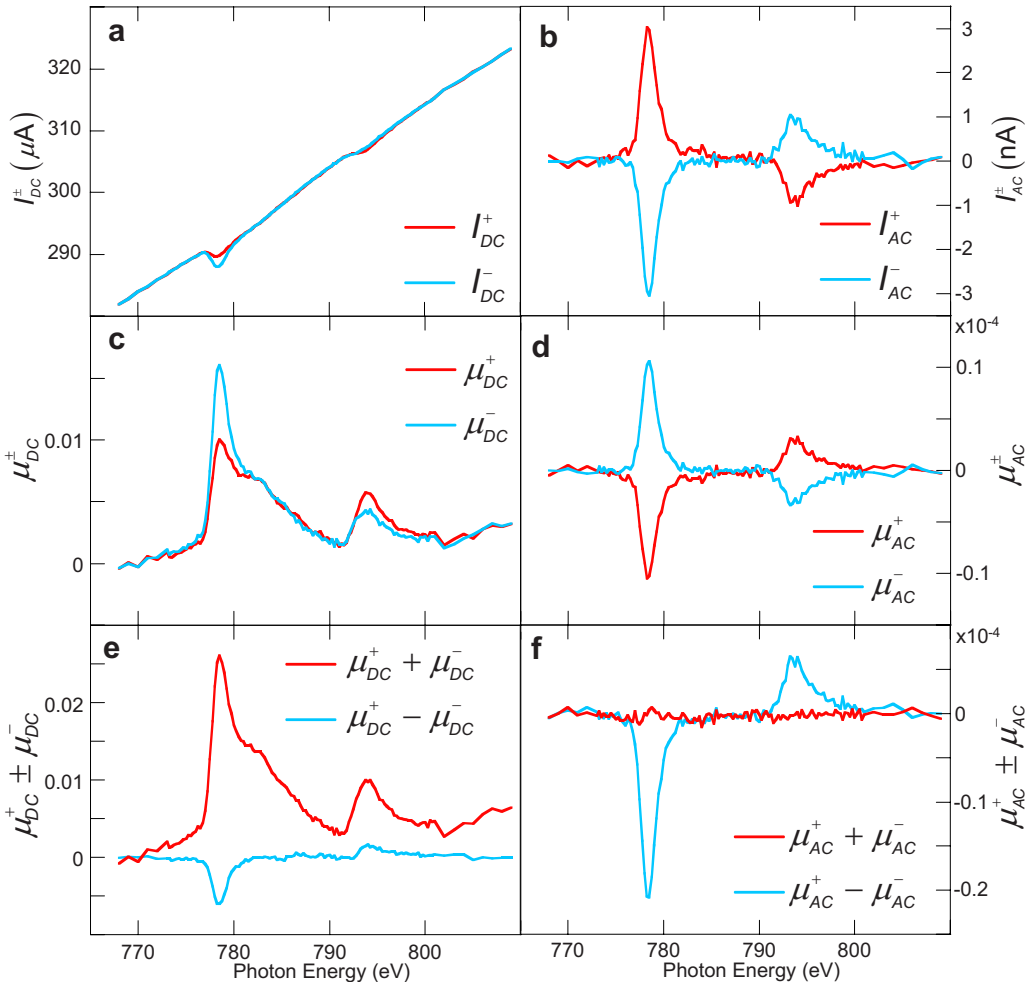

FIG. 3. (Color online) Energy scans at the L_2/L_3-edges of Co in ferromagnetic resonance condition ($B_0 \cong B_R \cong 0.64$ T). Average of ten scans per polarization, 5 min/scan, integration time of 0.1 s. Same notation as in Fig. 2.

on the nonresonant x-ray absorption of the sample. Consequently, the absorption values reported in Figs. 2–4 and in Table I are resonant x-ray absorptions values, with an accuracy limited by the difficulties in the determination of the background current I_b mentioned above.

As shown in Figs. 2–4, we have $\mu^{+}_{ac} \cong -\mu^{-}_{ac}$ for all three atoms and, consequently, $(\mu^{+}_{ac}+\mu^{-}_{ac}) \ll (\mu^{+}_{ac}-\mu^{-}_{ac})$. In terms of the basic model developed in Sec. II, this means that $(\mathrm{Re}[\sigma_{xx}]-\mathrm{Re}[\sigma_{zz}]) \ll \mathrm{Im}[\sigma_{xy}]$. This is in contrast with the behavior observed at the L_2/L_3-edges of Fe in $Y_3Fe_5O_{12}$, where $(\mu^{+}_{ac}+\mu^{-}_{ac}) \sim (\mu^{+}_{ac}-\mu^{-}_{ac})$ (see Ref. 3 and 16).

The relatively small but nonzero value of $(\mu^{+}_{ac}+\mu^{-}_{ac})$ is not due to experimental artifacts. An energy shift problem can be excluded because (1) the energy shift between plus and minus circular polarization is below 0.02 eV, (2) inverting the order of the scans with plus and minus circular polarization we observe no variations in the results, and (3) performing scans with linearly polarized light we observe that $(\mu^{x}_{ac}+\mu^{y}_{ac}) \cong (\mu^{+}_{ac}+\mu^{-}_{ac})$ as expected from Eq. (6). The $(\mu^{+}_{ac}+\mu^{-}_{ac})$ spectrum therefore reflects the line shape of the small magnetic linear dichroism of Fe and Ni in Permalloy, which is hardly measurable using standard methods due to signal-to-noise ratio limitations.

As shown in Fig. 5, the ac and dc dichroisms have approximately the same energy dependence, i.e., the ratio $(\mu^{+}_{dc}-\mu^{-}_{dc})/(\mu^{+}_{ac}-\mu^{-}_{ac})$ is nearly energy independent. This is in agreement with the results of Eq. (10), where this ratio is shown to depend on the angle θ only. Additionally, the ratio $(\mu^{+}_{dc}-\mu^{-}_{dc})/(\mu^{+}_{ac}-\mu^{-}_{ac})$ is, within $\pm 4\%$, the same for the three atoms (see Table I). From Eq. (10), we obtain that $\theta \cong \sqrt{\pi(\mu^{+}_{ac}-\mu^{-}_{ac})/(\mu^{+}_{dc}-\mu^{-}_{dc})} \cong 6°$.

The tiny differences in the energy dependence between $(\mu^{+}_{dc}-\mu^{-}_{dc})$ and $(\mu^{+}_{ac}-\mu^{-}_{ac})$ visible in Fig. 5, might be due to the difficult determination of background current I_b, which for Co (and, to a minor extent, also for Fe) is not accurately described by a straight line. A difference between the dc and ac dichroism would be in contradiction with our simple model and, more importantly, it might imply different values for the orbital and spin components of the angular momentum as determined by the sum rules[27] applied to the dc and ac dichroism. A detailed analysis and discussion about the application of the sum rules to the x-ray detection of ferromagnetic resonance will be carried out in a forthcoming article.

Table I reports the measured currents and absorption values at the L_3-peaks for the three investigated atoms. The measured effective absorption coefficients $\mu^{\mathrm{eff}}_{a}=[(\mu^{+}_{dc}$

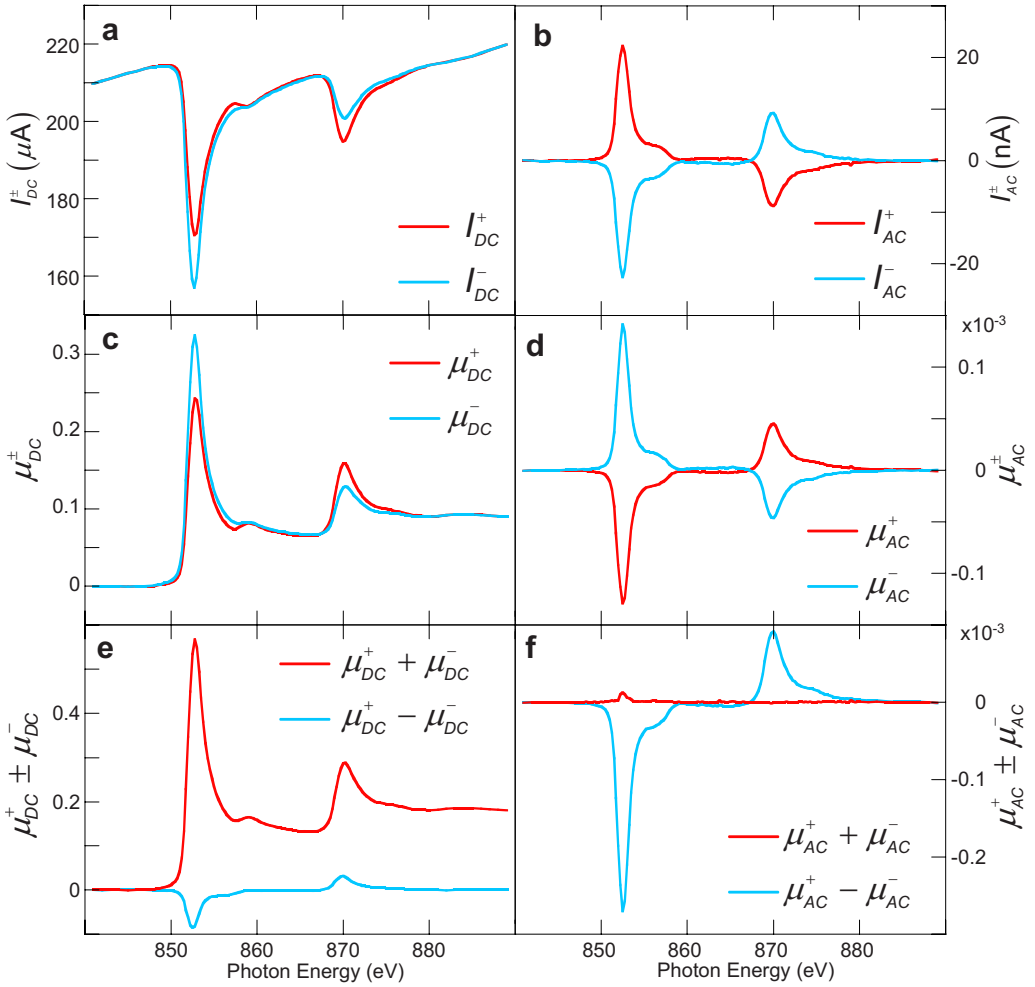

FIG. 4. (Color online) Energy scans at the L_2/L_3-edges of Ni in ferromagnetic resonance condition ($B_0 \cong B_R \cong 0.64$ T). Average of two scans per polarization, 12 min/scan, integration time of 3 s. Same notation as in Fig. 2.

$+\mu^{-}_{dc})/2](100/C)(1/t_s)$ corresponds, within a factor of 2, to the value of the absorption coefficients μ_a of pure Fe (bcc), Co (hpc), Ni (fcc) reported in Ref. 27, where C is the concentration (i.e., 73 for Ni, 18 for Fe, and 2 for Co for our $Ni_{73}Fe_{18}Gd_7Co_2$ sample).

The signal-to-noise ratio in the $\mu^{+}_{ac}-\mu^{-}_{ac}$ spectra is better than in the $\mu^{+}_{dc}-\mu^{-}_{dc}$ spectra, in spite of its much smaller absolute value (about a factor of 300, see Table I). This is mainly due to the immunity to low frequency noise of the ac measurements. The Co signal comes from the equivalent of about 1.3 monolayers. Since its amplitude $I^{\pm}_{ac}$ is about 3 nA and the noise is about 0.14 nA/$\sqrt{\text{Hz}}$, we have an element-specific ferromagnetic resonance sensitivity of the order of 0.1 monolayers/$\sqrt{\text{Hz}}$. Although we have submonolayer sensitivity, the absolute ferromagnetic resonance spin sensitivity is about 3×10^{10} spins/$\sqrt{\text{Hz}}$, which is not a particularly good spin sensitivity with respect to nonelement-resolved techniques.[28,29]

TABLE I. Absolute values of the photocurrent and absorption measured at the maximum of the L_3-edge magnetic dichroism.

	Units	Fe	Co	Ni
I_b	μA	280	290	220
$I^{+}_{dc}+I^{-}_{dc}-2I_b$	μA	86	4.5	105
$I^{+}_{dc}-I^{-}_{dc}$	μA	26	1.7	14
$I^{+}_{ac}-I^{-}_{ac}$	nA	88	6	45
$N_{rms}/\sqrt{\Delta f}$	nA/$\sqrt{\text{Hz}}$	0.13	0.12	0.13
$\text{SNR} \equiv I^{\pm}_{ac}/(N_{rms}/\sqrt{\Delta f})$	$\sqrt{\text{Hz}}$	340	20	180
$\mu^{+}_{dc}+\mu^{-}_{dc}$	1	0.36	0.026	0.56
$\mu^{+}_{dc}-\mu^{-}_{dc}$	1	0.11	0.006	0.084
$\mu^{+}_{ac}-\mu^{-}_{ac}$	10^{-3}	0.37	0.021	0.27
$(\mu^{+}_{dc}-\mu^{-}_{dc})/(\mu^{+}_{ac}-\mu^{-}_{ac})$	1	297	286	311
μ^{eff}_{a}	10^{-2} nm^{-1}	6.6	4.3	2.5
μ_a [a]	10^{-2} nm^{-1}	5.8	5.6	4.0

[a]From Ref. 27.

Figure 6 shows the ac absorption and ac dichroism as a function of the applied static magnetic field (B-scans), with photon energy fixed to the maximum of the dichroism. The absolute ac dichroism in Fig. 6(d) reflects the relative concentration, absorption cross section, and dc dichroism asymmetry of the three elements. In the normalized spectra shown in Fig. 6(e), we observe that (1) the three B-scans have approximately the same line shape and (2) the resonant fields are shifted by less than 3 mT, i.e., by less than 0.5% at the magnetic field of 640 mT. As the absolute flux of the x-ray beam decreases monotonically from Fe to Ni by approximately a factor of 2 due to the reduced intensity of the first undulator harmonic, it is possible that beam-induced heating

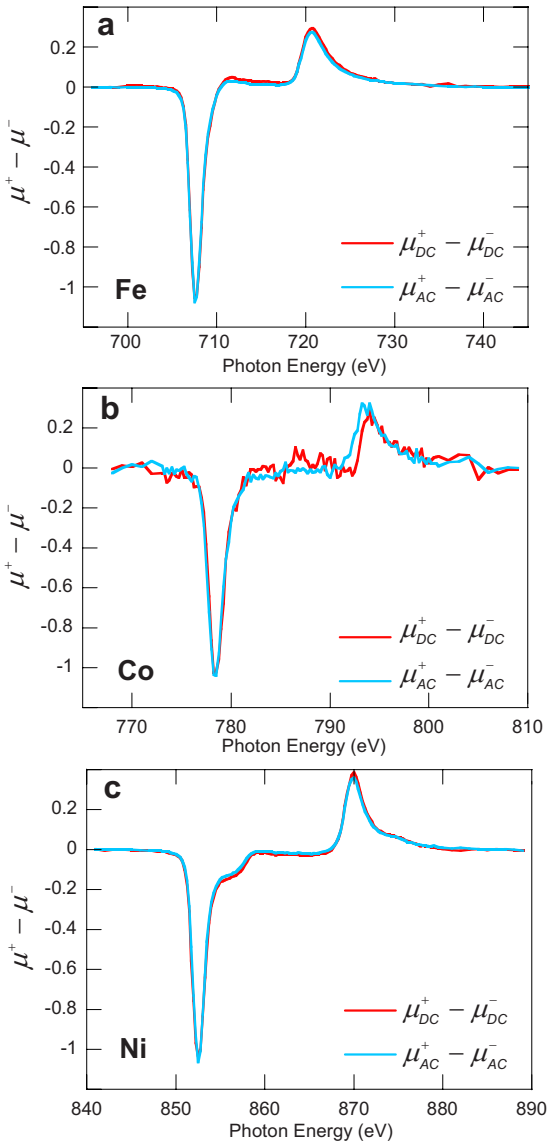

FIG. 5. (Color online) Comparison between the dc and ac dichroisms at the L_2/L_3-edges of (a) Fe, (b) Co, and (c) Ni in ferromagnetic resonance condition (i.e., $B_0 \cong B_R \cong 0.64$ T). The amplitudes have been normalized to 1 at the L_3-edge dichroism maximum.

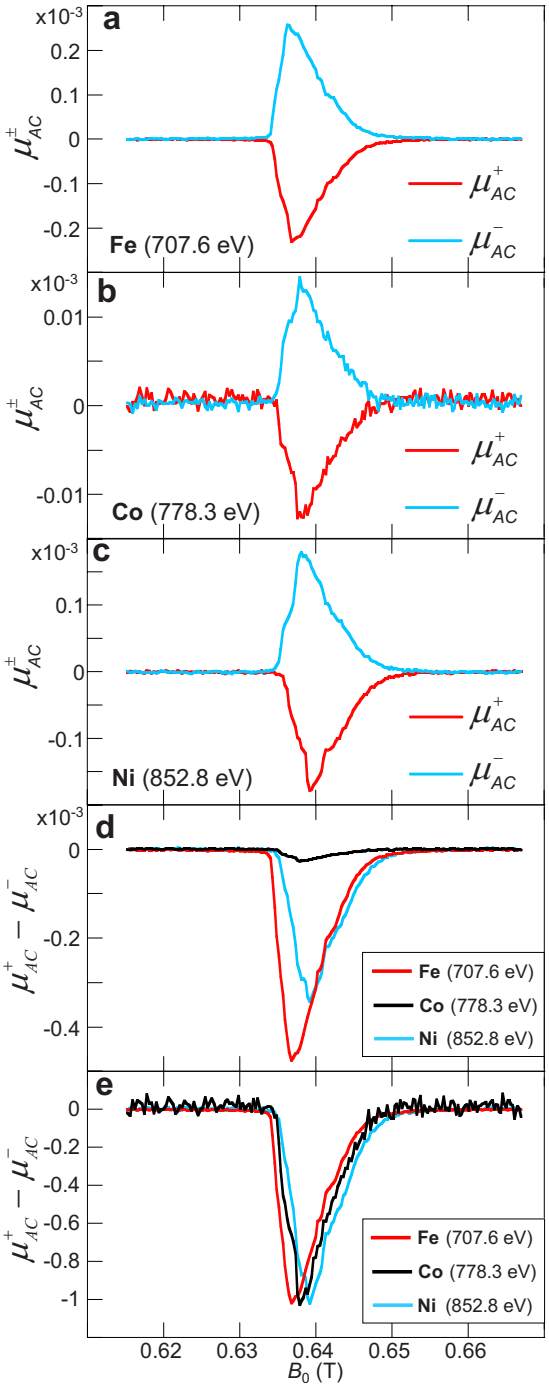

FIG. 6. (Color online) Static magnetic field scans (B-scans) at fixed photon energy corresponding to the L_3-edge dichroism maximum. ac absorption of (a) Fe, (b) Co, and (c) Ni. Comparison of the ac dichroisms: (d) absolute values and (e) amplitudes normalized to 1. One scan per polarization, 53 s/scan, integration time of 0.1 s.

is at the origin of such a shift. However, further experiments are required to elucidate this point. The asymmetric line shape of the B-scans might be due to the high power nonlinear excitation of spin waves, since the opening of the precession cone is close to the critical angle of the Suhl instability in Permalloy.[30,31]

The Gd signal has not been investigated in details because of the significantly reduced photon flux available at the Gd M_4/M_5-edges ($\sim$1.2 keV).

The currents ($I^{\pm}_{\mathrm{dc}}$, $I^{\pm}_{\mathrm{ac}}$) as well as the dichroisms ($I^{+}_{\mathrm{dc}} - I^{-}_{\mathrm{dc}}$, $I^{+}_{\mathrm{ac}} - I^{-}_{\mathrm{ac}}$) measured in transmission with the Al(160 nm)/Ta(2 nm)/$Ni_{73}Fe_{18}Gd_7Co_2$(15 nm)/Ta(2 nm)/Si_3N_4(200 nm) sample investigated in this work are approximately three orders of magnitude larger than the currents measured on the same sample, without the Al layer, using our fluorescence yield setup described in Refs. 3 and 13. This is essentially due to the fact that the fluorescence photodiode covers a fraction of solid angle ($\Omega/4\pi$) of about 0.2, and that at the L_3/L_2-edges of Fe, Co, and Ni the fluorescence yield (i.e., the number of fluorescence photons per absorbed photon) is about 0.01. In both situations the noise is limited by the shot noise $\sqrt{2QI_b\Delta f}$. Consequently, the signal-to-noise ratio in our transmission experiments is approximately 30 times better than in fluorescence measurements. However, as discussed in Ref. 32, the signal-to-noise ratio in transmission is not necessarily better than in fluorescence, especially for ultrathin samples or for highly diluted species in a weakly absorbing medium.

VI. CONCLUSIONS AND OUTLOOK

The experiments performed in this work demonstrate the possibility and underline the advantages of detecting the ferromagnetic resonance phenomenon using x-ray transmission measurements in the longitudinal configuration. A simple theoretical framework has been elaborated to analyze circularly and linearly polarized x-ray absorption spectra recorded simultaneously with resonant MW excitations. Factors limiting the signal-to-noise ratio and accuracy of the measurements have been discussed in detail, showing that it is possible to achieve an equivalent resolution of 0.1 monolayers/$\sqrt{\text{Hz}}$ at the L_3/L_2-edges of the transition metals.

An interesting question concerns the possibility to perform element-specific ferromagnetic resonance measurements with nanometer scale spatial resolution. With the last generation of scanning transmission x-ray microscopes (STXM),[1,5,27,33,34] a photon flux $I_s \sim 10^8$ photons/s can be focused down to about 20×20 nm^2. As an example, with a sample of $Ni_{80}Fe_{20}$ at the L_3/L_2-edges, we have $\mu_t \sim \mu_a \sim 10^{-2}$ nm^{-1}. From Eq. (12), assuming $\delta\mu_a \sim 0.001\mu_a$ and $t_s \sim 20$ nm, one has that SNR $\sim 1\sqrt{\text{Hz}}$. This means that with state-of-the art STXM element-resolved ferromagnetic resonance experiments in highly concentrated samples with 20 nm spatial resolution should be feasible. However, for diluted atoms and/or for the scanning of many pixels in a reasonably short time, significant improvements in the photon flux density (with possible problems of radiation damage) and/or $\delta\mu_a$ are required. As an alternative to STXM, lensless Fourier transform holography[27,35] could be used, which does not require beam focusing and, at least in principle, has a spatial resolution limited only by the x-ray wavelength (i.e., about 1.5 nm at 800 eV).

A potentially very interesting extension of the technique would be the x-ray detection of paramagnetic resonance. We have already attempted it, without success, on a single crystal of MnF_2 in fluorescence at the L_3/L_2 of Mn, working at 300 K and with a 9 GHz MW field. The broad resonance line (about 50 mT), the small spin polarization at 300 K, and the low fluorescence yield (about 0.01) are probably the main reasons of our unsuccessful first attempt. At low temperature, relatively strong XMCD signals have been already measured in paramagnetic systems at the L_3/L_2-edges of Mn, Fe, Co, and Ni.[36–41] Working at low temperatures and/or with samples having narrower paramagnetic resonance lines and, eventually, in transmission instead of fluorescence, element-resolved paramagnetic resonance studies might become feasible.

ACKNOWLEDGMENTS

Part of this work has been performed at the Swiss Light Source, Paul Scherrer Institut, Switzerland. Financial support from the European Research Council (Starting Grant No. 203239) and the Spanish Ministerio de Ciencia e Innovación (Grant No. HA2007-0098) is gratefully acknowledged. We are grateful to E. Fullerton, E. Shipton, and K. Chan of the University of California San Diego for letting us use their deposition system and for assisting in the sample preparation.

APPENDIX: TRANSVERSAL X-RAY DETECTION OF FMR

In Sec. II we have shown that, with a circularly polarized beam propagating along the magnetization precession direction (i.e., $\mathbf{k} \| \hat{\mathbf{z}}$), the MW-induced variation of the magnetization component along $\hat{\mathbf{z}}$ is measured analogously to a longitudinally detected ferromagnetic resonance experiment. Here we assume that the x-ray beam is propagating along the $\hat{\mathbf{y}}$-direction (i.e., $\mathbf{k} \| \hat{\mathbf{y}}$), with the magnetization precessing about the $\hat{\mathbf{z}}$-axis as in Sec. II. In these conditions, a transversal time-resolved detection of the magnetization precession with circularly polarized light is possible. In our model, for $\mathbf{k} \| \hat{\mathbf{y}}$, we have

$$\mathbf{E}^+ = -E(1/\sqrt{2})\exp(i\omega_{XR}t)(\hat{\mathbf{x}} + i\hat{\mathbf{z}}),$$

$$\mathbf{E}^- = E(1/\sqrt{2})\exp(i\omega_{XR}t)(\hat{\mathbf{x}} - i\hat{\mathbf{z}}), \tag{A1}$$

and

$$\begin{aligned}\mu^+ &= \alpha \sin\theta \sin\varphi \,\mathrm{Im}[\sigma_{xy}] + \alpha(1/8)[(5\text{-}\cos 2\theta \\ &\quad -2\cos 2\varphi \sin^2\theta)\mathrm{Re}[\sigma_{xx}] + (3 + \cos 2\theta \\ &\quad + 2\cos 2\varphi \sin^2\theta)\mathrm{Re}[\sigma_{zz}]], \\ \mu^- &= -\alpha \sin\theta \sin\varphi \,\mathrm{Im}[\sigma_{xy}] + \alpha(1/8)[(5\text{-}\cos 2\theta \\ &\quad -2\cos 2\varphi \sin^2\theta)\mathrm{Re}[\sigma_{xx}] + (3 + \cos 2\theta \\ &\quad + 2\cos 2\varphi \sin^2\theta)\mathrm{Re}[\sigma_{zz}]],\end{aligned} \tag{A2}$$

which gives

$$\begin{aligned}(\mu^+ - \mu^-) &= \alpha 2 \sin\theta \sin\varphi \,\mathrm{Im}[\sigma_{xy}], \\ (\mu^+ + \mu^-) &= \alpha(1/4)[(5\text{-}\cos 2\theta\text{-}2\cos 2\varphi \sin^2\theta)\mathrm{Re}[\sigma_{xx}] \\ &\quad + (3 + \cos 2\theta + 2\cos 2\varphi \sin^2\theta)\mathrm{Re}[\sigma_{zz}]].\end{aligned} \tag{A3}$$

Since the absorption $\mu^{\pm}$ depends on the azimuthal precession angle φ, it contains a component at frequency ω_{MW}. Due to the photon bunch structure, the transmitted photon flux current contains terms at $(n\omega_{\mathrm{PB}} \pm \omega_{\mathrm{MW}})$. By setting $\omega_{\mathrm{MW}} = n\omega_{\mathrm{PB}}$ with the MW source phase-locked to the photon bunch repetition frequency, it is possible to obtain a dc component measurable by the photodiode. By introducing a variable time delay (i.e., a phase shift) between the MW excitation at ω_{MW} and the multiple of the photon bunch repetition frequency $n\omega_{\mathrm{PB}}$, the component at frequency ω_{MW} of the absorption $\mu^{\pm}$ can be measured. This corresponds to the equivalent-time time-resolved measurement of the magnetization precession, which has been experimentally demonstrated in Refs. 1, 2, 5, 6, 8, 9, 12, 14, and 15.

For small precession angles, we have $(\mu^+ - \mu^-) \propto \sin\theta \cong \theta$ for $\mathbf{k} \| \hat{\mathbf{y}}$ and $(\mu^+ - \mu^-) \propto \cos\theta \cong (1 - \theta^2)$ for $\mathbf{k} \| \hat{\mathbf{z}}$. This means that for $\mathbf{k} \| \hat{\mathbf{y}}$ the variation of the circular dichroism due to the ferromagnetic resonance is larger (by a factor of $1/\theta$) with respect to the condition $\mathbf{k} \| \hat{\mathbf{z}}$. However, in this configuration the "unperturbed" dichroism (i.e., the one

without MW excitation) is zero and, consequently, it cannot be measured simultaneously with the ferromagnetic resonance induced dichroism.

[1] H. Stoll, A. Puzic, B. van Waeyenberge, P. Fischer, J. Raabe, M. Buess, T. Haug, R. Hollinger, C. Back, D. Weiss, and G. Denbeaux, Appl. Phys. Lett. **84**, 3328 (2004).
[2] W. E. Bailey, L. Cheng, D. J. Keavney, C. C. Kao, E. Vescovo, and D. A. Arena, Phys. Rev. B **70**, 172403 (2004).
[3] G. Boero, S. Rusponi, P. Bencok, R. S. Popovic, H. Brune, and P. Gambardella, Appl. Phys. Lett. **87**, 152503 (2005).
[4] J. Goulon, A. Rogalev, F. Wilhelm, N. Jaouen, C. Goulon-Ginet, G. Goujon, J. Ben Youssef, and M. V. Indenbom, JETP Lett. **82**, 696 (2005).
[5] A. Puzic, B. Van Waeyenberge, K. W. Chou, P. Fischer, H. Stoll, G. Schutz, T. Tyliszczak, K. Rott, H. Bruckl, G. Reiss, I. Neudecker, T. Haug, M. Buess, and C. H. Back, J. Appl. Phys. **97**, 10E704 (2005).
[6] D. A. Arena, E. Vescovo, C. C. Kao, Y. Guan, and W. E. Bailey, Phys. Rev. B **74**, 064409 (2006).
[7] J. Goulon, A. Rogalev, F. Wilhelm, N. Jaouen, C. Goulon-Ginet, and C. Brouder, Eur. Phys. J. B **53**, 169 (2006).
[8] Y. Guan, W. E. Bailey, C. C. Kao, E. Vescovo, and D. A. Arena, J. Appl. Phys. **99**, 08J305 (2006).
[9] D. A. Arena, E. Vescovo, C. C. Kao, Y. Guan, and W. E. Bailey, J. Appl. Phys. **101**, 09C109 (2007).
[10] J. Goulon, A. Rogalev, F. Wilhelm, C. Goulon-Ginet, and G. Goujon, J. Synchrotron Radiat. **14**, 257 (2007).
[11] J. Goulon, A. Rogalev, F. Wilhelm, N. Jaouen, C. Goulon-Ginet, G. Goujon, J. Ben Youssef, and M. V. Indenbom, J. Electron Spectrosc. Relat. Phenom. **156–158**, 38 (2007).
[12] Y. Guan, W. E. Bailey, E. Vescovo, C. C. Kao, and D. A. Arena, J. Magn. Magn. Mater. **312**, 374 (2007).
[13] G. Boero, S. Mouaziz, S. Rusponi, P. Bencok, F. Nolting, S. Stepanow, and P. Gambardella, New J. Phys. **10**, 013011 (2008).
[14] T. Martin, G. Woltersdorf, C. Stamm, H. A. Dürr, R. Mattheis, C. H. Back, and G. Bayreuther, J. Appl. Phys. **103**, 07B112 (2008).
[15] T. Martin, G. Woltersdorf, C. Stamm, H. A. Dürr, R. Mattheis, C. H. Back, and G. Bayreuther, J. Appl. Phys. **105**, 07D310 (2009).
[16] G. Boero, S. Rusponi, P. Bencok, R. Meckenstock, J. U. Thiele, F. Nolting, and P. Gambardella, Phys. Rev. B **79**, 224425 (2009).
[17] D. A. Arena, Y. Ding, E. Vescovo, S. Zohar, Y. Guan, and W. E. Bailey, Rev. Sci. Instrum. **80**, 083903 (2009).
[18] J. B. Kortright and S.-K. Kim, Phys. Rev. B **62**, 12216 (2000).
[19] C. Kittel, Phys. Rev. **73**, 155 (1948).
[20] N. Bloembergen and S. Wang, Phys. Rev. **93**, 72 (1954).
[21] H. Ebert, Rep. Prog. Phys. **59**, 1665 (1996).
[22] H. S. Bennett and E. A. Stern, Phys. Rev. **137**, A448 (1965).
[23] J. Goulon, A. Rogalev, G. Goujon, C. Gauthier, E. Moguiline, A. Sole, S. Feite, F. Wilhelm, N. Jaouen, C. Goulon-Ginet, P. Dressler, P. Rohr, M. O. Lampert, and R. Henck, J. Synchrotron Radiat. **12**, 57 (2005).
[24] F. Scholze, H. Rabus, and G. Ulm, J. Appl. Phys. **84**, 2926 (1998).
[25] J. D. Spear, Rev. Sci. Instrum. **76**, 076101 (2005).
[26] C. T. Chen, Y. U. Idzerda, H. J. Lin, N. V. Smith, G. Meigs, E. Chaban, G. H. Ho, E. Pellegrin, and F. Sette, Phys. Rev. Lett. **75**, 152 (1995).
[27] J. Stöhr and H.-C. Siegmann, *Magnetism* (Springer, Berlin, 2006).
[28] M. Farle, Rep. Prog. Phys. **61**, 755 (1998).
[29] O. Klein, G. Loubens, V. V. Naletov, F. Boust, T. Guillet, H. Hurdequint, A. Leksikov, A. N. Slavin, V. S. Tiberkevich, and N. Vukadinovic, Phys. Rev. B **78**, 144410 (2008).
[30] A. J. Berteaud and H. Pascard, J. Appl. Phys. **37**, 2035 (1966).
[31] H. M. Olson, P. Krivosik, K. Srinivasan, and C. E. Patton, J. Appl. Phys. **102**, 023904 (2007).
[32] P. A. Lee, P. H. Citrin, P. Eisenberger, and B. M. Kincaid, Rev. Mod. Phys. **53**, 769 (1981).
[33] W. L. Chao, B. D. Harteneck, J. A. Liddle, E. H. Anderson, and D. T. Attwood, Nature (London) **435**, 1210 (2005).
[34] J. Raabe, G. Tzvetkov, U. Flechsig, M. Boge, A. Jaggi, B. Sarafimov, M. G. C. Vernooij, T. Huthwelker, H. Ade, D. Kilcoyne, T. Tyliszczak, R. H. Fink, and C. Quitmann, Rev. Sci. Instrum. **79**, 113704 (2008).
[35] S. Eisebitt, J. Luning, W. F. Schlotter, M. Lorgen, O. Hellwig, W. Eberhardt, and J. Stohr, Nature (London) **432**, 885 (2004).
[36] J. Van Elp, S. J. George, J. Chen, G. Peng, C. T. Chen, L. H. Tjeng, G. Meigs, H. J. Lin, Z. H. Zhou, M. W. W. Adams, B. G. Searle, and S. P. Cramer, Proc. Natl. Acad. Sci. U.S.A. **90**, 9664 (1993).
[37] T. Funk, P. Kennepohl, A. J. Di Bilio, W. A. Wehbi, A. T. Young, S. Friedrich, E. Arenholz, H. B. Gray, and S. P. Cramer, J. Am. Chem. Soc. **126**, 5859 (2004).
[38] P. Gambardella, S. S. Dhesi, S. Gardonio, C. Grazioli, P. Ohresser, and C. Carbone, Phys. Rev. Lett. **88**, 047202 (2002).
[39] P. Gambardella, H. Brune, S. S. Dhesi, P. Bencok, S. R. Krishnakumar, S. Gardonio, M. Veronese, C. Grazioli, and C. Carbone, Phys. Rev. B **72**, 045337 (2005).
[40] H. Brune and P. Gambardella, Surf. Sci. **603**, 1812 (2009).
[41] P. Gambardella, S. Stepanow, A. Dmitriev, J. Honolka, F. M. F. de Groot, M. Lingenfelder, S. Sen Gupta, D. D. Sarma, P. Bencok, S. Stanescu, S. Clair, S. Pons, N. Lin, A. P. Seitsonen, H. Brune, J. V. Barth, and K. Kern, Nature Mater. **8**, 189 (2009).